

Determining parameters of a spherical black hole with thin accretion disk by observing its shadow

Kenta Hioki^{1,*} and Umpei Miyamoto^{2,†}

¹*Sumitomo Mitsui Banking Corporation, 1-2,
Marunouchi 1-chome, Chiyoda-ku, Tokyo 100-0005, Japan^a*

²*Research and Education Center for Comprehensive Science,
Akita Prefectural University, Akita 015-0055, Japan*

Abstract

We revisit the classic system of a spherically symmetric black hole in general relativity (*i.e.*, a Schwarzschild black hole) surrounded by a geometrically thin accretion disk. Our purpose is to examine whether one can determine three parameters of this system (*i.e.*, black hole mass M ; distance between the black hole and an observer r_o ; inclination angle i) solely by observing the accretion disk and the black-hole shadow. A point in our analysis is to allow r_o to be finite, which is set to be infinite in most relevant studies. First, it is shown that one can determine the values of $(r_o/M, i)$, where M/r_o is the so-called angular gravitational radius, from the size and shape of shadow. Then, it is shown that if one additionally knows the accretion rate \dot{M} (resp. mass M) by any independent theoretical or observational approach, one can determine the values of (M, r_o, i) [resp. (\dot{M}, r_o, i)] without degeneracy, in principle, from the value of flux at any point on the accretion disk.

PACS numbers: 04.20.-q, 04.20.Cv, 04.70.-s

^a The statements expressed in this paper are those of the authors and do not represent the views of Sumitomo

Mitsui Banking Corporation or its staff.

* kenta.hioki@gmail.com

† umpei@akita-pu.ac.jp

I. INTRODUCTION

Black holes are quite interesting objects and provide us an ultimate test ground of strong gravitational fields. Therefore, it had been a mark to observe the shadow of a black hole forming when the light rays emitted from the ambient material is bent by the gravitational field of black hole.

Recently, the shadow of M87, which had been a black hole candidate, was indeed observed by an Earth-size very long baseline interferometer (VLBI) [1–7], and that of Sgr A* was observed too [8–13]. One method to confirm the existence of black holes by observing the shadow can be said to be established (but see also [14]).

One might say that the study of black-hole imaging was started with the derivation of shadow contour or, as we now call it, apparent shape. The apparent shape of a Schwarzschild black hole was first derived in [15], and that of a Kerr black hole was done in [16]. These works should be said to establish the basis of the shadow theory. While they considered simple ‘bare’ black holes, namely, did not take into account accretion disks around the black holes, the role of photon sphere was revealed, which plays a central role even in the shadow of black hole with the accretion disk.

The image of Schwarzschild black hole with the accretion disk was derived in [17]. The image of Kerr black hole with the accretion disk was done in [18, 19] for several fixed values of parameter. The numerical study of shadow using the models that can be thought to mimic real situations also made remarkable progress [20]. The apparent shapes and images of various black-hole solutions have also been obtained [21–29].

In spite of the above extensive studies, we would like to say that a comprehensive or sufficient analysis of the apparent shape and image of black-hole candidates has not been performed yet. In particular, it remains to be examined whether it is possible or not to extract information such as the angular momentum of black hole by observing the shadow.

One method to examine the above possibility is to investigate whether or not a map from a parameter space to an image library is an injection [30]. One of the present author (K.H.) and his collaborator, based on this idea, showed that the map from the parameter space to the apparent-shape library for a bare Kerr black hole is indeed a bijection, which means that the angular momentum (per mass squared) and inclination angle of the Kerr black hole can be determined by observing its apparent shape. Here, the apparent-shape library is defined

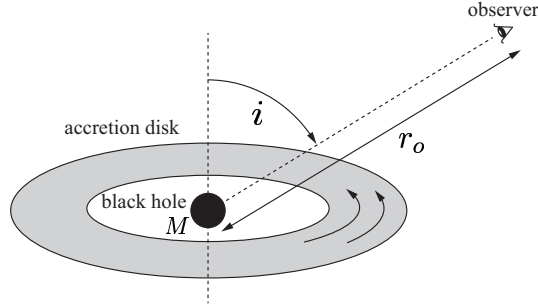


FIG. 1. A schematic picture showing three parameters (M, r_o, i) of the system considered in this paper. M (> 0) is the mass of a Schwarzschild black hole surrounded by an infinitely thin rotating accretion disk. An observer is located at distance $r_o \in [20M, +\infty)$ from the center of black hole in the geometrical units ($c = G = 1$). Inclination angle $i \in [0^\circ, 90^\circ)$ is defined as the angle between the rotation axis of the accretion disk and observer. The distance of the inner and outer edges of accretion disk from the center of black hole are $6M$ (*i.e.*, the innermost stable circular orbit) and $20M$, respectively. The results in this paper are independent of the position of outer edge.

as the set of all possible apparent shapes that can be generated in the given gravitational theory and model.

Subsequently, the observables of black-hole shadows which characterize the shadow were improved [31] and geometric analysis of the apparent shapes was developed [32]. Using the improved observables and actual data, an attempt was made to identify the black-hole solution describing M87 and to put restrictions on its physical parameters [33].

Is it possible to (i) confirm that it is a black hole, (ii) identify the black-hole solution, and (iii) determine its physical quantities only by observing the shadow image of a black-hole candidate object? To answer these questions, we presumably have to conduct laborious research. Namely, we have to prepare a huge amount of models of relativistic objects and accretion disks, and construct their image libraries by allowing their parameters to change. Then, we also have to investigate whether the map is injective (or invertible). If it is not injective, it means that there exists an image corresponding to different models and parameter settings, and it will be impossible to determine the model based on shadow observation alone. These efforts are currently in progress, and further studies are required.

In this paper, as a first step to answer the above questions, we reinvestigate the classic model of the Schwarzschild black hole with the thin accretion disk considered in Ref. [17],

from a different point of view. Namely, we allow the distance between the black hole and the observer to be *finite* rather than infinite. The reason is that we expect a large number of black-hole candidates to be observed in future, all of which are at different distances from us, and we would like to present a method taking into account finite-distance effects precisely. The three parameters characterizing our simple system are shown in Fig. 1. Note that a few methods to take into account the finite-distance effects in shadow observation were proposed [34, 35].

As the results, we will see that one can determine only the angular gravitational radius M/r_o and inclination angle i from the observation of apparent shape of shadow. We will see, however, that one can determine the mass M , distance r_o , and inclination angle i separately if the value of bolometric energy flux at any point on the accretion disk is observed, and if the value of accretion rate \dot{M} is known from any independent theoretical or observational approach.

The organization of this paper is as follows. In Sec. II, we briefly review the behaviors of null and timelike geodesics around a Schwarzschild black hole, which correspond to the motion of the photons emitted from the accretion disk and massive particles in the accretion disk, respectively. In Sec. III, we describe the system in a correct manner, how to define two dimensional image from the null geodesics, and how to determine the system's parameters from observation. In Sec. IV, we present the results on the apparent shape of black hole obtained by using the formulation prepared in previous sections. It is shown that one can determine the values of $(r_o/M, i)$ by observing the size and shape of shadow. In Sec. V, it is shown that further observational information, *i.e.*, the flux at any point on the accretion disk and the mass accretion rate, makes it possible to determine the values of (M, r_o, i) without degeneracy. We summarize our analysis and mention future prospects in the final section. We use the geometrical units, in which $c = G = 1$, throughout this paper.

II. GEODESICS IN SCHWARZSCHILD SPACETIME

The line element in the Schwarzschild black hole is

$$g_{\mu\nu}(x)dx^\mu dx^\nu = -f(r)dt^2 + \frac{1}{f(r)}dr^2 + r^2(d\theta^2 + \sin^2\theta d\phi^2), \quad f(r) := 1 - \frac{2M}{r}, \quad (1)$$

where $x^\mu = (t, r, \theta, \phi)$ ($\mu, \nu = 0, 1, 2, 3$) and $M (> 0)$ is the mass of black hole. The geodesic equations for a massless particle and a massive particle is obtained as the Euler-Lagrange

equation

$$\frac{d}{d\lambda} \left(\frac{\partial \mathcal{L}}{\partial \dot{x}^\mu} \right) - \frac{\partial \mathcal{L}}{\partial x^\mu} = 0, \quad (2)$$

with a respective suitable Lagrangian \mathcal{L} . Here, the dot represents the derivative with respect to λ , parametrizing the geodesic $x^\mu(\lambda)$.

A. Null geodesics

The Lagrangian for a massless particle on equatorial plane $\theta = \pi/2$ is

$$\mathcal{L} = \frac{1}{2} g_{\mu\nu} \frac{dx^\mu}{d\lambda} \frac{dx^\nu}{d\lambda} = -\frac{1}{2} f(r) \dot{t}^2 + \frac{1}{2} f(r)^{-1} \dot{r}^2 + \frac{1}{2} r^2 \dot{\phi}^2. \quad (3)$$

From t and ϕ components of Euler-Lagrange equation (2) with Lagrangian (3), we obtain

$$p_t = -f(r) \dot{t} = -E, \quad p_\phi = r^2 \dot{\phi} = L, \quad (4)$$

where $p_\mu := \frac{\partial \mathcal{L}}{\partial \dot{x}^\mu}$, and E and L are integration constants. In the case of a massless particle, λ is an affine parameter. Combining Eq. (4) with null condition $\mathcal{L} = 0$, we obtain

$$\left(\frac{dr}{d\lambda'} \right)^2 = 1 - \frac{b^2 f(r)}{r^2}, \quad (5)$$

where $\lambda' := E\lambda$, and $b := L/E$ is an impact parameter. Substituting Eqs. (4) and (5) into chain rule $\frac{dr}{d\phi} = \frac{dr}{d\lambda'} \frac{d\lambda'}{d\phi}$, we obtain the equation for trajectory $r = r(\phi)$ in a potential form,

$$\left(\frac{1}{r^2} \frac{dr}{d\phi} \right)^2 + V(r) = \frac{1}{b^2}, \quad V(r) := \frac{f(r)}{r^2}. \quad (6)$$

As shown in Fig. 2, effective potential $V(r)$ has a maximum $V(3M) = 1/(27M^2) =: 1/b_c^2$, where $r = 3M$ is the photon sphere. According to [36], we call a null geodesic with impact parameter b larger than $b_c = 3\sqrt{3}M$ that of *the first kind*, and call a null geodesic with impact parameter b smaller than b_c that with *an imaginary eccentricity*. These two kinds of geodesics, both of which play central roles in our analysis, can reach sufficiently far region (namely, an observer), provided they are emitted outwards from a point with $r > 3M$.

If one considers a geodesic moving outwards ($\frac{dr}{d\phi} > 0$) from $r = r_1$ to $r = r_2$ ($r_1 < r_2$), the change of ϕ during such a motion is obtained by integrating Eq. (6),

$$\phi(r_2) - \phi(r_1) = \int_{r_1}^{r_2} \frac{b}{r \sqrt{r^2 - b^2 f(r)}} dr. \quad (7)$$

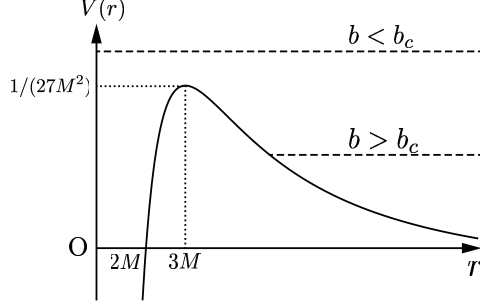


FIG. 2. A schematic picture of effective potential $V(r)$ for a massless particle around the Schwarzschild black hole [see Eq. (6)]. Two horizontal dashed lines represent lines of $1/b^2$. The lower line ($b > b_c := 3\sqrt{3}M$) and upper line ($b < b_c$) correspond to the null geodesic of the first kind and with an imaginary eccentricity, respectively.

As we will see in the next section, the captured image of accretion disk is made by both the geodesics of the first kind and with imaginary eccentricity. For both kinds of geodesics, the integral in Eq. (7) can be written down in terms of the incomplete elliptic integrals of the first kind.

B. Timelike geodesics

The Lagrangian for a massive particle moving on equatorial plane $\theta = \pi/2$ is

$$\mathcal{L}_m = \frac{1}{2}m g_{\mu\nu} \frac{dx^\mu}{d\tau} \frac{dx^\nu}{d\tau} = -\frac{1}{2}m f(r) \dot{t}^2 + \frac{1}{2}m f(r)^{-1} \dot{r}^2 + \frac{1}{2}m r^2 \dot{\phi}^2, \quad (8)$$

where m (> 0) is the mass of particle, and the dot represents the derivative with respect to particle's proper time τ here. From t and ϕ components of Euler-Lagrange equation (2) with Lagrangian (8), we obtain

$$m f(r) \dot{t} = E_m, \quad m r^2 \dot{\phi} = L_m, \quad (9)$$

where E_m and L_m are integration constants. Combining Eq. (9) with normalization condition $g_{\mu\nu} \dot{x}^\mu \dot{x}^\nu = -1$, we obtain the equation of radial motion in a potential form,

$$\left(\frac{dr}{d\tau} \right)^2 + U(r) = \frac{E_m^2}{m^2}, \quad U(r) := \left(1 + \frac{L_m^2}{m^2 r^2} \right) f(r). \quad (10)$$

The behavior of effective potential $U(r)$ depends on the angular momentum L_m . For a particle with a relatively large angular momentum, characterized by $L_m > L_c := 2\sqrt{3}mM$,

$U(r)$ has critical points at $r = r_{\pm}$ ($3M < r_- < 6M < r_+$), where $r = r_-$ and $r = r_+$ correspond to unstable and stable circular orbits, respectively (see Fig. 3). For $L_m = L_c$, r_- and r_+ coincide to be $6M$, which is the radius of *innermost stable circular orbit* (ISCO). For $L_m < L_c$, both critical points do not exist.

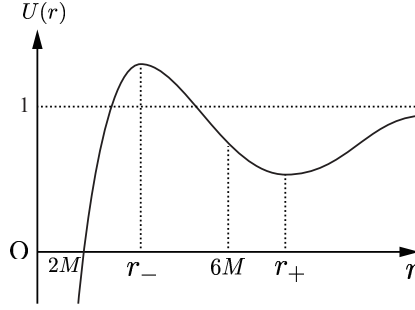


FIG. 3. A schematic picture of effective potential $U(r)$ for a massive particle around the Schwarzschild black hole, which depends on angular momentum of particle L_m [see Eq. (10)]. As in this picture, the potential has critical points at $r = r_-$ and $r = r_+$ ($3M < r_- < 6M < r_+$) for $L_m > L_c := 2\sqrt{3}mM$. In the limit of $L_m \rightarrow L_c + 0$, the both critical points approach $6M$, which corresponds to the position of ISCO.

The angular velocity of a particle Ω is given by

$$\Omega = \frac{\dot{\phi}}{\dot{t}} = \frac{L_m f(r)}{E_m r^2}, \quad (11)$$

where we have used Eq. (9) in the last equality. Now, let us consider a perfectly circular orbit or a Keplerian motion. The radius of such an orbit (namely, r_+) is determined by two conditions of $U(r) = E_m^2/m^2$ and $U'(r) = 0$. Eliminating from E_m and L_m from the right-hand side of Eq. (11) using these two conditions, we can represent the angular velocity of the Keplerian motion in terms of its radius,

$$\Omega = \sqrt{\frac{M}{r^3}}. \quad (12)$$

It is well known that this result coincides with one obtained from a Newtonian argument, namely the balance between gravitational force Mm/r^2 and centrifugal one $mr\Omega^2$.

We will assume all particles in the accretion disk to be in the Keplerian motion. Then, from Eq. (12), closer to the center the angular velocity is greater, namely the rotation is differential one. Therefore, the inner material exerts a torque on the outer material in the direction of rotation through viscous stresses. Such viscous stresses transport angular

momentum outward through the disk. The material that loses angular momentum spirals gradually inward until $r = 6M$ (ISCO), and finally falls into the black hole. The viscous stresses, working against the differential rotation, also play the role of heating the disk to cause it to emit a large amount of flux [37].

III. SETUP

Although the system of the black hole, accretion disk, and observer we investigate in this paper is quite simple as shown in Fig. 1, let us describe it little more precisely here. Then, let us explain how to define two dimensional image of the subject (*i.e.*, the accretion disk) from the information encoded in the null rays emitted from it. This is indispensable because the shape and size of image may depend on the definition of two dimensional image, in particular, when the subject is close to the observer. Finally, we will define a map from a parameter space to the set of images, which is necessary for later investigation.

A. Black hole surrounded by an accretion disk and observer

The positions of the black hole, accretion disk, and observer are schematically shown in Fig. 4(a). In this figure, a unit sphere of which center O coincides with that of the Schwarzschild black hole is drawn. Here, we introduce Schwarzschild coordinates $(t, r, \bar{\theta}, \bar{\phi})$ by letting its origin $r = 0$ coincide with O in Fig. 4(a). While we identify coordinates (t, r) with those in Eq. (1), let us stress that coordinates $(\bar{\theta}, \bar{\phi})$, which are related to (X, Y, Z) in the standard way, are *independent* of (θ, ϕ) in Eq. (1) at this point.

In terms of the Schwarzschild coordinates introduced above, the accretion disk, which is an optically thick rotating annulus, is on the equatorial plane $\bar{\theta} = \pi/2$, and its inner and outer edges are at $r = 6M$ (ISCO) and $r = 20M$, respectively. The observer rests at O' of which position is specified by $(r, \bar{\theta}, \bar{\phi}) = (r_o, i, \pi/2)$. Here, r_o and i are in the range of $20M \leq r_o < \infty$ and $0 \leq i < \pi/2$, respectively. A photon emitted by a massive particle in the accretion disk at E', of which coordinates are $(r, \bar{\theta}, \bar{\phi}) = (r_e, \pi/2, \pi/2 - \psi)$, reaches the observer along the null geodesic E'O'. Needless to say, r_e and ψ are assumed to be in the range of $6M \leq r_e \leq 20M$ and $0 \leq \psi < 2\pi$, respectively. We stress that the position of outer edge of accretion disk, $r = 20M$, has no special meaning in the sense that the conclusion in

this paper does not depend on this assumption.

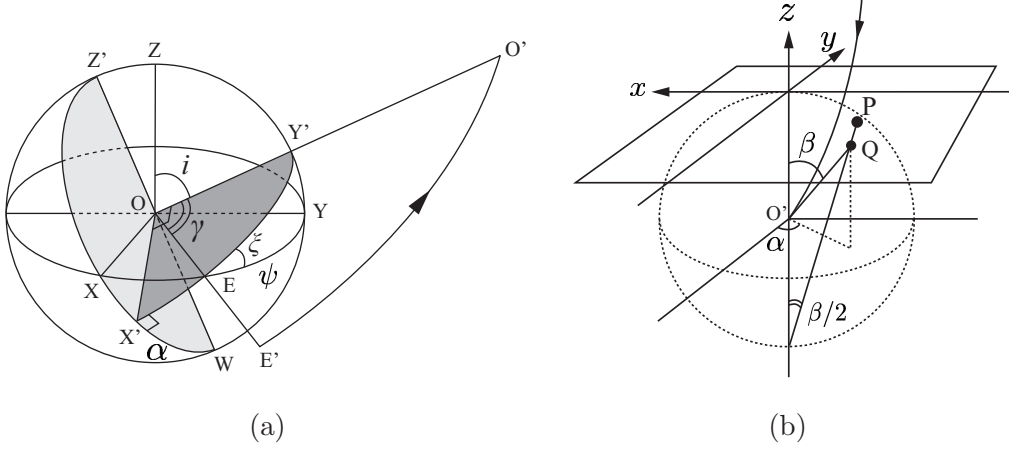


FIG. 4. (a) A schematic picture showing a unit sphere of which center O coincides with that of the Schwarzschild black hole. The observer is located at O' , which is on $X = 0$ plane. The accretion disk, which is a rotating annulus, is on the $Z = 0$ plane. A null ray emitted at E' by a massive particle in the accretion disk reaches the observer along null ray $E'O'$. See the text for the detail. (b) A schematic picture showing a unit celestial sphere for the observer O' . z -axis points the center of black hole O . (α, β) is a celestial coordinate system, which is used to specify the incident angle of the null ray into the observer. Q is the point where the tangent of null ray at O' crosses the unit sphere. P is the two dimensional image made by the null ray.

As mentioned before, all particles in the accretion disk are assumed to be in the Keplerian motion (*i.e.*, a perfectly circular orbit). We also assume that every particle in the accretion disk isotropically radiates null rays in all directions. Among such null rays, only ones with appropriate impact parameter b can reach the observer to generate the image, and the rest null rays either fall into the black hole or escape to the asymptotic region. The shadow of black hole is defined as the region in the two dimensional image where no null ray reaches and which is surrounded by the image of accretion disk. The apparent shapes of black hole and accretion disk are defined by a boundary of a black-hole shadow and a boundary of an accretion-disk image, respectively.

For simplicity, we consider only the primary image, which is generated by primary rays, in this paper. Namely, we do not consider the secondary and higher images, generated by the photons that have circled the black hole once or more before reaching the observer.

B. How to define two dimensional image

We have to relate the information about the null rays to the two dimensional image of accretion disk in a way that works even when r_o is finite. As such a method, in this paper, we employ a stereographic projection from a celestial sphere onto a plane [34]. Note that the “local shadow” proposed in Ref. [35] is different from ours. Our notations here are similar to ones in [17].

A unit celestial sphere for the observer O' is drawn in Fig. 4(b). In this figure, z -axis points the center of black hole O . We define the celestial coordinates (α, β) as in Fig. 4(b), by which the incident angle of photon into the observer are specified. Note that angle α in Fig. 4(b) corresponds to $\alpha = \angle X'OW$ in Fig. 4(a), which is determined by the positions of the observer and emitting particle, *i.e.*, by i and ψ [see Eqs. (14) and (15)].

Applying the law of sines in the spherical trigonometry to the spherical triangles EXX' and EYY' , we have

$$\frac{\sin(\pi/2)}{\sin(\pi/2 - \psi)} = \frac{\sin \xi}{\sin(\pi/2 - \alpha)}, \quad \frac{\sin \xi}{\sin(\pi/2 - i)} = \frac{\sin(\pi/2)}{\sin \gamma}. \quad (13)$$

Here, $\xi = \angle Y'EY'$ and $\gamma = \angle EOO'$. For simplicity, let us call γ the deflection angle, while the standard deflection angle in gravitational lensing phenomena corresponds to $\pi - 2\gamma$. Eliminating ξ from two relations in Eq. (13), one obtains

$$\cos \alpha = \frac{\cos \psi \cos i}{\sin \gamma}. \quad (14)$$

Another relation among angles we need is

$$\cos \gamma = \sin i \cos \psi, \quad (15)$$

which is obtained by the following elementary geometric consideration. First, if one draws a perpendicular from Y' to OE and call its foot H , $OH = \cos \gamma$. Next, if one draws a perpendicular from Y' to OY and call its foot K , $\triangle HKY'$ is a right triangle with $\angle HKY' = \pi/2$. Using this fact, one can represent OH in another way, as $OH = \sin i \cos \psi$. Thus, we obtain relation (15).

Eliminating ψ from Eqs. (14) and (15), one obtains

$$\cos \alpha = \cot i \cot \gamma. \quad (16)$$

In order to calculate γ , we identify the equatorial plane $\theta = \pi/2$ in the Schwarzschild coordinates of Eq. (1) with plane OX'Y' in Fig. 4(a), and further identify ϕ in Eq. (1) with the angle of photon's position measured from OX'. After this identification, we set

$$r_1 = r_e, \quad \phi(r_1) = \frac{\pi}{2} - \gamma, \quad r_2 = r_o, \quad \phi(r_2) = \frac{\pi}{2} \quad (17)$$

in Eq. (7). Then, we obtain

$$\gamma = \int_{r_e}^{r_o} \frac{b}{r \sqrt{r^2 - b^2 f(r)}} dr. \quad (18)$$

Thus, using Eqs. (16) and (18), we obtain the one of the incident angle, α , as a function of i, M, r_o, r_e , and b .

Now, let get down to the rest incident angle, β . The tangent of β is given by

$$\tan \beta = \frac{p_{(\phi)}}{p_{(r)}} \bigg|_{(r, \theta) = (r_o, \pi/2)}, \quad (19)$$

where $p_{(a)} := e_{(a)}^\mu p_\mu$ ($a = t, r, \theta, \phi$) is the tetrad component of the photon's momentum. Tetrad basis $e_{(a)}$ is given by

$$e_{(t)} = \frac{1}{\sqrt{f(r)}} \partial_t, \quad e_{(r)} = \sqrt{f(r)} \partial_r, \quad e_{(\theta)} = \frac{1}{r} \partial_\theta, \quad e_{(\phi)} = \frac{\csc \theta}{r} \partial_\phi. \quad (20)$$

Note that $w := e_{(t)}|_{r=r_o}$ is also the four-velocity of observer. Using Eqs. (4), (5), (19), (20), and the fact of $p_r = \frac{\partial \mathcal{L}}{\partial \dot{r}} = f(r)^{-1} \dot{r}$, we obtain

$$\tan \beta = \sqrt{\frac{b^2 f(r_o)}{r_o^2 - b^2 f(r_o)}}. \quad (21)$$

Thus, we obtain β as a function of M, r_o , and b .

As in Fig. 4(b), point Q on the unit celestial sphere, specified by (α, β) , is projected onto point P on the plane (a photographic plate) specified by (x, y) in a stereographic way [34]. The relation between these coordinates are

$$x = -2 \sin \alpha \tan \frac{\beta}{2}, \quad y = -2 \cos \alpha \tan \frac{\beta}{2}. \quad (22)$$

A circle with radius 2 in the x - y plane corresponds to the celestial equator.

Here, let us give a comment. We consider a *unit* celestial sphere (namely, a sphere of dimensionless radius) just for simplicity. In reality, however, we should consider a celestial sphere of a dimensionful radius ℓ (say). Then, the right-hand sides in Eq. (22) have factor ℓ ,

and therefore the size of image in x - y plane is proportional to ℓ . Here, it would be natural to think ℓ to correspond roughly to the size of observational apparatus.

In summary, we can obtain the two dimensional image of accretion disk (therefore, also the black-hole shadow and apparent shape of black hole) using Eqs. (16), (21), and (22) for a fixed values of (M, r_o, i) by changing (r_e, b) within the whole range allowed.

C. Map from the parameter space to apparent-shape library

For our purpose to examine whether one can determine the parameters of (black hole) + (accretion disk) + (observer) system by observation, it is convenient to define a parameter space \mathcal{P} , an apparent-shape library \mathcal{J} (letter \mathcal{J} stands for Image), and a map $\Psi : \mathcal{P} \rightarrow \mathcal{J}$ [30].

Parameter space \mathcal{P} in our problem is a subset of \mathbb{R}^3 of which element is a direct product of three parameters $\{M\}$, $\{r_o\}$, and $\{i\}$,

$$\mathcal{P} := \{(M, r_o, i) \mid M > 0, r_o \geq 20M, 0 \leq i < \pi/2\} \subset \mathbb{R}^3. \quad (23)$$

For later convenience, we also define an equivalence relation \sim in \mathcal{P} by

$$(M, r_o, i) \sim (M', r'_o, i') \stackrel{\text{def.}}{\iff} \begin{cases} r_o/M = r'_o/M' \\ i = i' \end{cases}. \quad (24)$$

Map Ψ is defined to map $(M, r_o, i) \in \mathcal{P}$ to an apparent shape in the way described in the final paragraph of Sec. IIIB. Then, apparent-shape library \mathcal{J} is defined as the image of Ψ as $\mathcal{J} := \Psi(\mathcal{P})$, namely a collection of all apparent shapes that the present (black hole) + (accretion disk) + (observer) system generates in the prescribed way.

While map Ψ is surjective by definition, it is not necessarily injective. If Ψ is not injective, an element in \mathcal{J} can correspond to two or more distinct elements in \mathcal{P} , which means that one cannot determine the parameters from an apparent shape. On the other hand, if Ψ is injective, Ψ is bijective or invertible so that one can always uniquely specify black-hole parameters $(M, r_o, i) \in \mathcal{P}$ corresponding to an apparent shape in \mathcal{J} , that is identical to (or approximating enough in reality) an actual observed apparent shape.

IV. SIZE AND SHAPE OF SHADOW

A. Deflection angle and images

What left before drawing the two dimensional image is to calculate the integral in γ [see Eq. (18)]. Although the integral cannot be written down in terms of elementary functions unfortunately at least in the case that r_o is infinite (see [36, p.132 and p.134]), it is known that the integral can be written down in terms of the incomplete elliptic integral of the first kind,

$$F(\Phi, K) := \int_0^\Phi \frac{d\vartheta}{\sqrt{1 - K^2 \sin^2 \vartheta}}. \quad (25)$$

As will be seen soon, this is the case also when r_o is finite.

It is convenient to introduce a parameter that labels the geodesics instead of impact parameter b . Such a parameter for the null geodesic of the first kind is the perihelion of orbit P , related to the impact parameter b by

$$b^2 = \frac{P^3}{P - 2M}, \quad P > 3M \quad (\Leftrightarrow b > b_c). \quad (26)$$

With this parameter, deflection angle γ in Eq. (18) for finite r_o is calculated to yield

$$\gamma = 2\sqrt{\frac{P}{Q}} \left[F(\zeta(r_e), k) - F(\zeta(r_o), k) \right]. \quad (27)$$

Here, all quantities in Eq. (27) are written in terms of (M, r_o, r_e, P) through

$$Q^2 := (P - 2M)(P + 6M), \quad k^2 := \frac{Q - P + 6M}{2Q}, \quad (28)$$

$$\sin^2 \zeta(r) := \frac{Q - P + 2M + 4MP/r}{Q - P + 6M}. \quad (29)$$

For the null geodesic with an imaginary eccentricity, a convenient parameter that labels the geodesics instead of impact parameter is μ defined by

$$b^2 = \frac{M^2}{\mu(4\mu - 1)^2}, \quad \mu > \frac{1}{3} \quad (\Leftrightarrow 0 < b < b_c). \quad (30)$$

With this parameter, deflection angle γ in Eq. (18) for finite r_o is calculated to yield

$$\gamma = \frac{1}{\sqrt{\Delta}} \left[F(\sigma(r_o), \kappa) - F(\sigma(r_e), \kappa) \right]. \quad (31)$$

All quantities in Eq. (31) are written in terms of (M, r_o, r_e, μ) through

$$e^2 := \frac{3\mu - 1}{\mu}, \quad \Delta^2 := 48\mu^2 - 16\mu + 1, \quad \kappa^2 := \frac{\Delta + 6\mu - 1}{2\Delta}, \quad (32)$$

$$\tan \frac{\xi(r)}{2} := \frac{1}{e} \left(\frac{M}{\mu r} - 1 \right), \quad \sin^2 \sigma(r) := \frac{\Delta - 2\mu e \sin \xi(r) - (6\mu - 1) \cos \xi(r)}{\Delta + 6\mu - 1}. \quad (33)$$

Substituting Eqs. (27) and (31) into Eq. (16), and using Eqs. (21) and (22), one can draw a two dimensional image for a given set of values (M, r_o, i) by changing $r_e \in [6M, 20M]$, P , and μ .

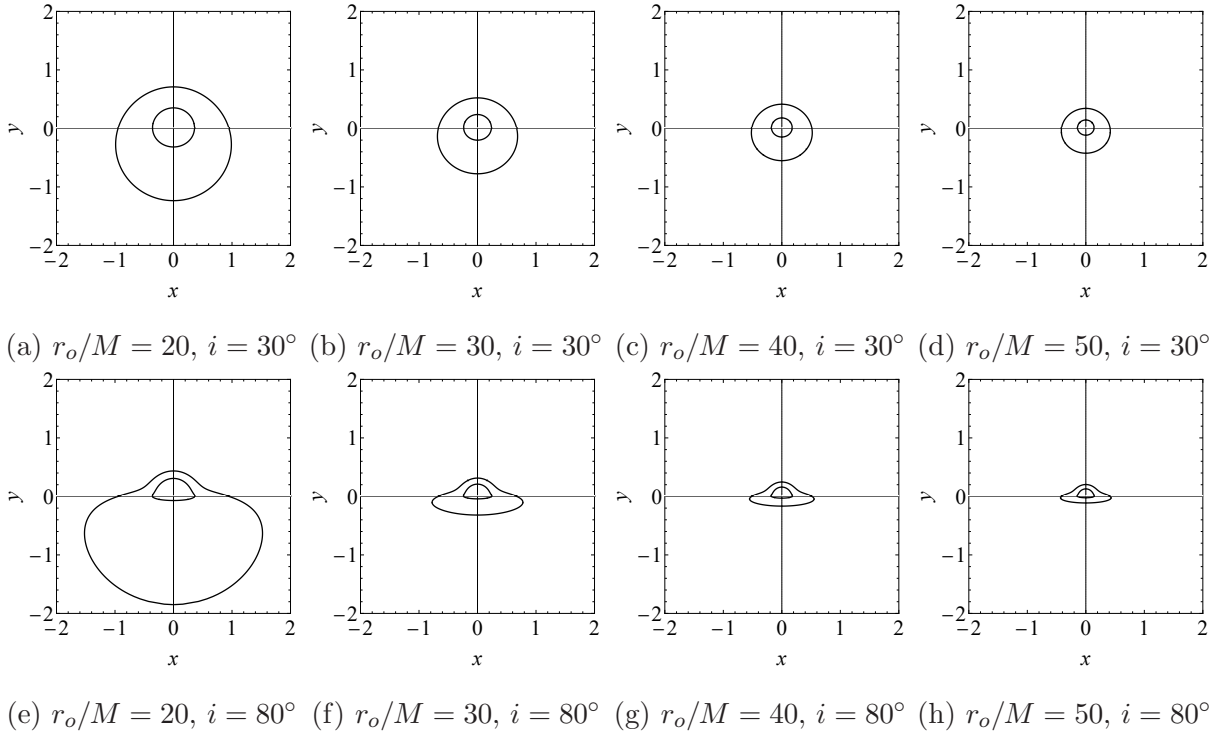


FIG. 5. Shadows of Schwarzschild black holes surrounded by thin accretion disks.

In Fig. 5, we present the images for two values of inclination angle $i = 30^\circ$ and 80° and four values of dimensionless distance $r_o/M = 20, 30, 40$, and 50 . In each figure, we only plot the apparent shape of the accretion disk, which is generated by the null rays emitted from the inner and outer edges of accretion disk. The inner boundary of the apparent shape of accretion disk is nothing but the apparent shape of black hole by definition.

When the inclination angle is small, we see that the disk seems like a slightly deformed annulus, which is the well known result [38], and the apparent size of such an annulus becomes small as r_o increases as expected.

Even when the inclination is large, the ‘opposite’ side of accretion disk far from the observer is always visible due to the strong deflection of light rays by the black hole, as well

known. What interesting happens when the inclination angle is large and r_o/M is close to 20. Namely, in such cases, the annulus is highly deformed. As far as the present authors know, such a highly deformed image is presented for the first time in this paper, which allows r_o to be finite.

The reason why we have presented the images in Fig. (5) for several values of r_o/M is that the size and shape depend on r_o/M , of which inverse is sometimes called the *angular gravitational radius*, rather than r_o and M themselves. This can be proved rigorously. Namely, the position of image (x, y) is the function of (M, r_e, r_o, i, b) (or P and μ instead of b) through Eqs. (16), (21), (22), (27), (31) and so on. However, if we normalize every dimensionful quantity by M as

$$r_{e*} := \frac{r_e}{M}, \quad r_{o*} := \frac{r_o}{M}, \quad b_* := \frac{b}{M}, \quad P_* := \frac{P}{M}. \quad (34)$$

The position of image (x, y) becomes the function of dimensionless quantities (i, r_{e*}, r_{o*}, b_*) (or P_* and μ instead of b_*) and does not depend on M explicitly. In other words, when $(r_o/M, i) = (r_o/M', i')$ holds, the image of system with (M, r_o, i) and that of system with (M', r'_o, i') are completely *congruent*.

From the above fact, we can say that all elements in an equivalence class $[(M, r_o, i)]$ of quotient space \mathcal{P}/\sim is mapped to an image or shape in \mathcal{J} by a map Ψ . This does not mean, however, that a map Ψ_q is injective, where Ψ_q is defined as $\Psi_q : \mathcal{P}/\sim \ni [(M, r_o, i)] \mapsto \Psi((M, r_o, i)) \in \mathcal{J}$. In the next subsection, we will show that $\Psi_q : \mathcal{P}/\sim \rightarrow \mathcal{J}$ is indeed injective, which means that one can determine value of $(r_o/M, i)$ by capturing image.

B. Size and shape determines $(r_o/M, i)$

Since the ISCO has a universal meaning as we saw in Sec. II B, we focus on the apparent shape of the black hole corresponding to the ISCO. Then, we will define two observables characterizing the apparent shape of the black hole [30].

We approximate the apparent shape of black hole by a circle passing through the three points located at the top position, the most left end, and the most right end of the shadow as in the three green points in Fig. 6. We denote the radius of this circle by R .

Next, let us consider the dent in the bottom part of the shadow. The size of the dent is denoted by D , which is the length between the bottom positions of circle and the shadow

as in Fig. 6. Then, we define the distortion parameter of the shadow by $\delta := D/R$.

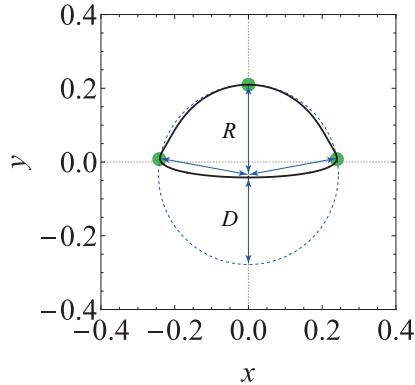


FIG. 6. The observables for the apparent shape of a Schwarzschild black hole surrounded by a thin disk are the radius R , being the radius of an approximating circle, and the distortion parameter $\delta := D/R$, where D is the difference between the down endpoints of the circle and of the shadow.

We present the contour plots of R and δ in Fig. 7(a) and (b), respectively. The contour plots of R and δ are overlayed in Fig. 8. From Fig. 7, we can see that R decreases as r_o/M increases, and δ increases as i increases, which we have already seen in Fig. 5. Note that the apparent shape is so distorted that δ exceeds 1 for $i \gtrsim 80^\circ$.

Here, the following two facts are important for our purpose.

- From Fig. 7(b), even when $i = \text{const.}$, $\delta \neq \text{const.}$
- From Fig. 8, there is a one-to-one correspondence between $(r_o/M, i)$ and (R, δ) .

The former means that two apparent shapes with distinct values of r_o/M are *not similar* even if the inclination angle i is common. The latter means that map $\Psi_q : \mathcal{P}/\sim \rightarrow \mathcal{J}$ is invertible (bijective). Therefore, if one measures R and δ by observations, the values of r_o/M and i are determined by using Fig. 8.

V. FLUX OF THE ACCRETION DISK

We have seen that information read from the apparent shape of shadow is insufficient to determine the parameters completely. Therefore, in this section, we utilize another observationally measurable quantity, *i.e.*, the energy flux emitted by the accretion disk, in order to make the parameter determination complete.

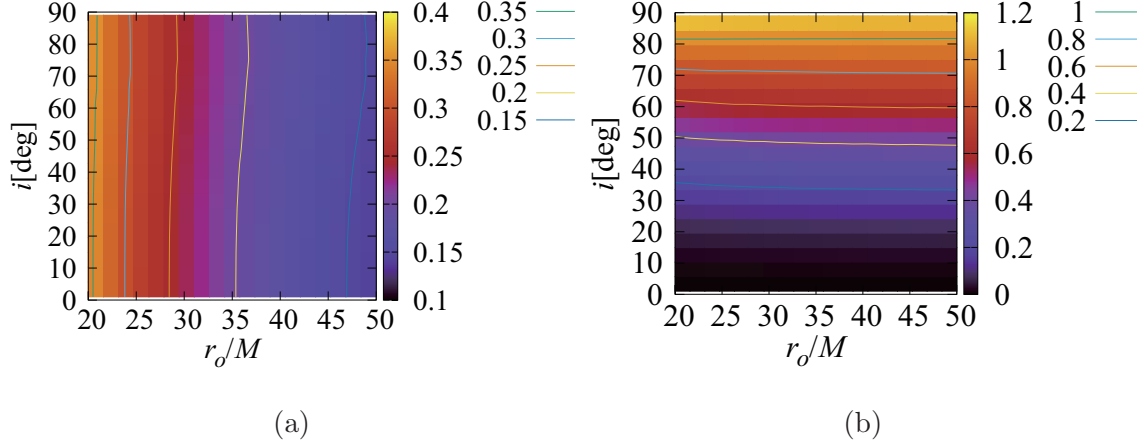


FIG. 7. (a) A contour map of the radii of shadow R of for the Schwarzschild black hole surrounded by the thin accretion disk. (b) A contour map of the distortion parameter δ .

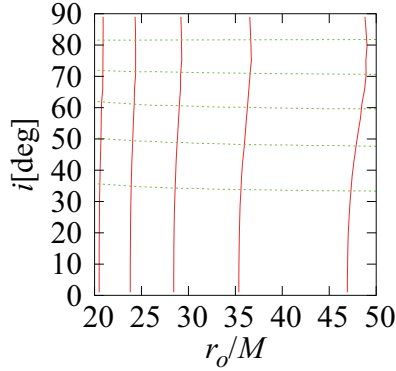


FIG. 8. The contours of the radius of shadow R (the red solid curves) and the distortion parameter δ (the green dashed curves). The contours are those for $R = 0.15, \dots, 0.35$, with the contour interval being 0.05, and $\delta = 0.2, \dots, 1$, with the contour intervals being 0.2, respectively.

A. Radial dependence of bolometric flux

Under quite general assumptions, Page and Thorne derived the radial dependence of energy flux radiated by a thin accretion disk around a stationary axially symmetric black hole in an explicit form [39, 40]. Restricting their general result to the present Schwarzschild case [17], the bolometric energy flux flowing out of the upper (or equally the lower) face of the accretion disk is given as a function of emitting point $r_{e*} = r_e/M$, by

$$F_e = \frac{3\dot{M}}{8\pi M^2} \frac{1}{(r_{e*} - 3)r_{e*}^{5/2}} \left(\sqrt{r_{e*}} - \sqrt{6} + \frac{\sqrt{3}}{2} \ln \left[\frac{(\sqrt{6} - \sqrt{3})(\sqrt{r_{e*}} + \sqrt{3})}{(\sqrt{6} + \sqrt{3})(\sqrt{r_{e*}} - \sqrt{3})} \right] \right), \quad (35)$$

where \dot{M} (> 0) is the radius-independent mass accretion rate. Note that the flux F_e of light emitted from ISCO is zero, as can be seen from Eq. (35). The bolometric flux F_o observed by an observer away from the disk differs from the above intrinsic flux F_e by the inverse fourth power of redshift factor $1 + z$ [41],

$$F_o = \frac{F_e}{(1 + z)^4}. \quad (36)$$

In the present case, the redshift and/or blueshift consists of the Doppler effect due to the motion of emitter and the gravitational redshift, which is given by

$$1 + z = \frac{-u^\mu p_\mu|_{r=r_e}}{-w^\mu p_\mu|_{r=r_o}}, \quad (37)$$

where u is the four velocity of emitting particle on the disk, and w is that of the observer at O' [see around Eq. (20)]. Note that the followings hold (see Sec. II).

$$(p_t, p_r, p_\theta, p_\phi) = (-E, f(r)^{-1} \sqrt{E^2 - f(r)L^2/r^2}, 0, L), \quad p_{\bar{\phi}} = p_\phi \cos \xi, \quad (38)$$

$$(u^t, u^r, u^{\bar{\theta}}, u^{\bar{\phi}}) = (u^t, 0, 0, \Omega u^t), \quad -1 = g_{\mu\nu} u^\mu u^\nu. \quad (39)$$

Substituting Eqs. (38) and (39) into Eq. (37) and using $\cos \xi = \sin i \sin \alpha$, which can be derived from Eqs. (13) and (15), we have the explicit form of redshift factor,

$$1 + z = \sqrt{\frac{1 - 2/r_{o*}}{1 - 3/r_{e*}}} \left(1 - \frac{b_*}{r_{e*}^{3/2}} \sin i \sin \alpha \right). \quad (40)$$

B. Map from the parameter space to image library

Now, we would like to upgrade the map from the parameter space to the apparent-shape library, $\Psi : \mathcal{P} \rightarrow \mathcal{J}$, to another map $\hat{\Psi} : \hat{\mathcal{P}} \rightarrow \hat{\mathcal{J}}$, in which not only the information about apparent shape but also that about the flux is involved.

First, we upgrade parameter space \mathcal{P} to $\hat{\mathcal{P}}$ by

$$\hat{\mathcal{P}} := \mathcal{P} \times \{\dot{M} \mid \dot{M} > 0\} \subset \mathbb{R}^4. \quad (41)$$

Next, we consider a set of all possible two dimensional images $\bar{\mathcal{J}}$, in which not only the information about the apparent shape of the black hole but also the information about the spatial distribution of bolometric flux on the accretion disk are contained. This set $\bar{\mathcal{J}}$ is regarded as the codomain of new map $\hat{\Psi}$. Namely, map $\hat{\Psi}$ is defined to map $(M, r_o, i, \dot{M}) \in \hat{\mathcal{P}}$ to an element (namely, a two dimensional image) in $\bar{\mathcal{J}}$.

Finally, $\hat{\mathcal{J}} \subset \bar{\mathcal{J}}$ is defined as the image of $\hat{\Psi}$ as $\hat{\mathcal{J}} := \hat{\Psi}(\hat{\mathcal{P}})$. Hereafter, we call $\hat{\mathcal{J}}$ the image library, which is a collection of all two dimensional images that the present (black hole) + (accretion disk) + (observer) system generates in the way described in Secs. III B and V A.

Remember that we change parameters P_* and μ within respective allowed range to plot the apparent shape of accretion disk in Fig. 5. Let $I \subset (3, r_e/M)$ and $J \subset (1/3, \infty)$ be such a range of P_* and μ , respectively. Then, map $\hat{\Psi}$ defined above can be written in a more specific way as,

$$\begin{aligned} \hat{\Psi} : (M, r_o, i, \dot{M}) &\in \hat{\mathcal{P}} \\ \mapsto \{(x, y, F_o) \mid P_* \in I, r_{e*} \in [6, 20]\} \sqcup \{(x, y, F_o) \mid \mu \in J, r_{e*} \in [6, 20]\} &\in \hat{\mathcal{J}}, \end{aligned} \quad (42)$$

where \sqcup stands for the disjoint union.

We also define an equivalence relation \approx in $\hat{\mathcal{P}}$ by

$$(M, r_o, i, \dot{M}) \approx (M', r'_o, i', \dot{M}') \stackrel{\text{def}}{\iff} \begin{cases} r_o/M = r'_o/M' \\ i = i' \\ \dot{M}/M^2 = \dot{M}'/M'^2 \end{cases}, \quad (43)$$

which will be used in the next subsection.

C. Flux determines (M, r_o, i)

We define a “blue-shifted flux” \mathcal{F} as an observable by

$$\mathcal{F} := \{(x, 0, F_o) \mid (x, y, F_o) \in \hat{\mathcal{J}}, x < 0, y = 0, F_o > 0\}, \quad (44)$$

which represents the x -dependence of observed flux F_o along the x -axis with $x < 0$. See the yellow part in Fig. 9. The reason why we focus on $x < 0$ region and call \mathcal{F} the blue-shifted flux is that the flux is blue-shifted (enhanced) on this side due to the rotational motion of accretion disk. Note that the origin and axes of (x, y) -coordinates can be identified by two observables (R, δ) .

We also define a dimensionless blue-shifted flux \mathcal{F}_* by

$$\mathcal{F}_* := \left\{ (x, 0, F_{o*}) \mid F_{o*} = \frac{M^2}{\dot{M}} F_o, (x, 0, F_o) \in \mathcal{F} \right\}, \quad (45)$$

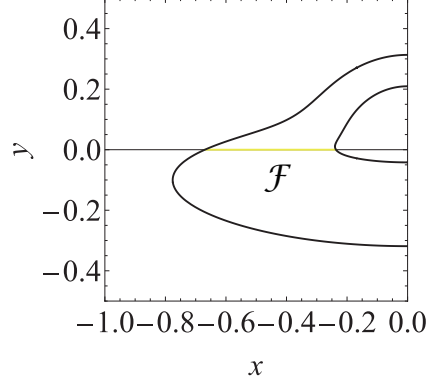


FIG. 9. Blue-shifted flux \mathcal{F} , representing the x -dependence of observed flux F_o along the x -axis

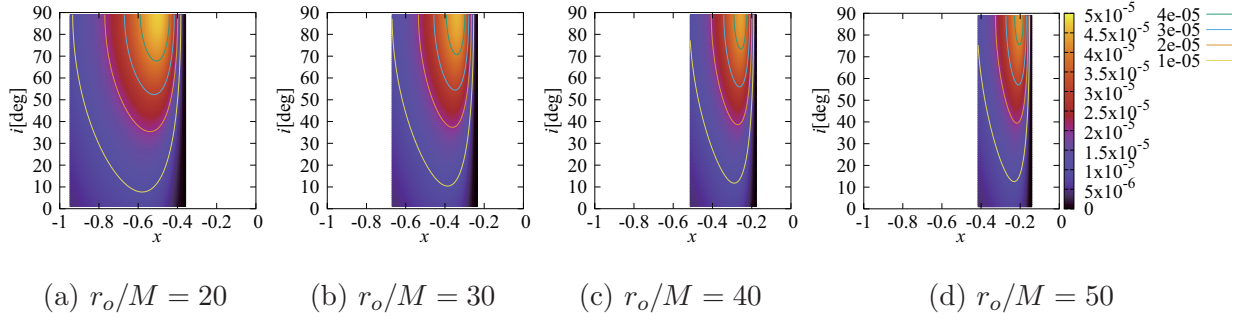


FIG. 10. Contour maps of dimensionless blue-shifted flux \mathcal{F}_* .

which represents the x -dependence of dimensionless flux F_{o*} along the x -axis with $x < 0$. The dependence of \mathcal{F}_* on i and r_o/M are shown in Fig. 10. A three dimensional plot is also given in Fig. 11.

Now, let us suppose the following situation.

- (i) From the observational measurement of (R, δ) , we have already known $(r_o/M, i)$ of the system.
- (ii) We have observed the bolometric energy flux to know F_o as a function of (x, y) or as a function of x on the x -axis with $x < 0$ at least.

Under assumptions (i) and (ii), parameters $(r_o/M, i, \dot{M}/M^2)$ can be determined only by capturing the two dimensional image. This is because the following relationship holds:

$$\frac{\dot{M}}{M^2} = \frac{F_o}{F_{o*}} \bigg|_{x < 0, y = 0}. \quad (46)$$

In other words, by observing the blue-shifted flux \mathcal{F} and using Figs. 10 and 11 we can determine \dot{M}/M^2 . Note that the right-hand side of Eq. (46) apparently has the dependence

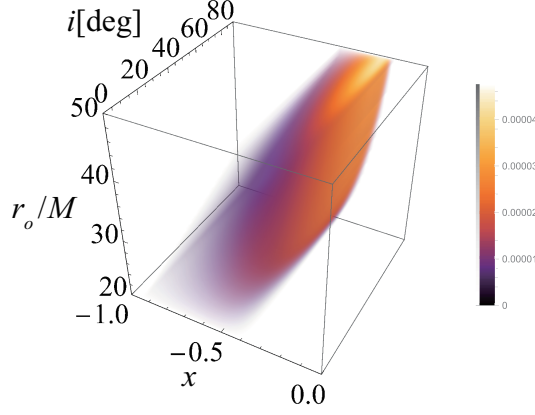


FIG. 11. The dependence of dimensionless blue-shifted flux \mathcal{F}_* on i and r_o/M .

on x but it is constant and thus the right-hand side can be evaluated at *any* point on the x -axis provided $x < 0$ and $F_o > 0$ at that point.

We can say that all elements in an equivalence class $[(M, r_o, i, \dot{M})]$ of quotient space $\hat{\mathcal{P}}/\approx$ is mapped to a two dimensional image in $\hat{\mathcal{J}}$ by a map $\hat{\Psi}$. From the fact that the map Ψ_q is bijective and Eq. (46) holds, a map $\hat{\Psi}_q$ is bijective, where $\hat{\Psi}_q$ is defined as $\hat{\Psi}_q : \hat{\mathcal{P}}/\approx \ni [(M, r_o, i, \dot{M})] \mapsto \hat{\Psi}((M, r_o, i, \dot{M})) \in \hat{\mathcal{J}}$. Namely, there exist a one-to-one correspondence between $\hat{\mathcal{P}}/\approx$ and $\hat{\mathcal{J}}$, and we can determine the parameters of the system, $(r_o/M, i, \dot{M}/M^2)$, only by capturing the two dimensional image.

Furthermore, we suppose the following situation.

- (iii) With any independent theoretical or observational approach, we know accretion rate \dot{M} of the system.

Under three assumptions (i), (ii), and (iii), we can estimate mass M .

In summary, we can say that it is possible to determine the parameters of the system, (M, r_o, i) , by capturing the two dimensional image and from the information on the mass accretion rate. Note that if M is known (instead of \dot{M}), it is possible to determine \dot{M} .

D. Demonstration

Let us demonstrate how one obtains the value of M from an observational data. Reviving c and G in Eq. (45), we have

$$F_{o*} = \frac{G^2 M^2}{c^6 \dot{M}} F_o. \quad (47)$$

We assume that accretion rate \dot{M} is ϵ (a dimensionless factor) times the critical or Eddington accretion rate \dot{M}_E , namely, $\dot{M} = \epsilon \dot{M}_E := \epsilon L_E / c^2$, where L_E is the Eddington luminosity, given by

$$L_E = \frac{4\pi c G m_p}{\sigma_T} M, \quad \sigma_T = \frac{8\pi}{3} \left(\frac{e^2}{4\pi\epsilon_0 m_e c^2} \right)^2. \quad (48)$$

Here, σ_T is the cross section of Thomson scattering. Then, from Eq. (47) the mass is expressed as

$$M = \epsilon \cdot \frac{4\pi c^5 m_p}{G M_\odot \sigma_T F_o} \cdot F_{o*} M_\odot \simeq \epsilon \cdot \frac{5.76 \times 10^{25} \text{ erg/cm}^2/\text{s}}{F_o} \cdot F_{o*} M_\odot. \quad (49)$$

Suppose we have measured (R, δ) from the apparent shape of the black hole and gotten $(r_o/M, i) = (20, 30^\circ)$ by the method described in Sec. IV B. Furthermore, we know that $\epsilon = 0.01$ by any independent approach and observationally know that flux F_o on x -axis takes a maximum as $(x, y, F_o) = (-5.494 \times 10^{-1}, 0, 1.536 \times 10^9 \text{ erg/cm}^2/\text{s}) \in \mathcal{F}$. On the other hand, theoretical value of F_{o*} at the same position can be obtained by calculation as $(x, y, F_{o*}) = (-5.494 \times 10^{-1}, 0, 1.745 \times 10^{-5}) \in \mathcal{F}_*$ (see Fig. 10). Substituting these values into the right-hand side of Eq. (49), we obtain $M \simeq 6.548 \times 10^9 M_\odot$.

VI. CONCLUSION

We have analyzed the shadow of the Schwarzschild black hole with a thin accretion disk. In the analysis, the mass of black hole M and inclination angle i are assumed to be unknown, and the distance from the black hole to the observer r_o is assumed to be finite and unknown. The dependence of black-hole shadow shape and flux on mass M , distance r_o , and inclination angle i was investigated.

It was found that two black-hole shadows are congruent if r_o/M and i are common between the two systems. However, even though the shadows are congruent, the information about the flux can be used to distinguish such two systems. Any two systems can be distinguished from each other if both the shadow shape and flux information are observationally obtained, under the assumption one knows mass accretion rate \dot{M} independently.

In this paper, we have considered the Schwarzschild black hole surrounded by thin accretion disk for simplicity. The next step would be to consider more general black holes such as the Kerr black hole and more realistic models of accretion disks. The reversibility of the

map from the parameter space to the image library should be examined in such realistic models. If the image library is extended to include various black-hole solutions as models, and if a shadow image not included in such a image library is actually observed, it suggests the existence of new black-hole solution or the modification of gravitational theory.

Finally, it would be challenging but interesting to construct a movie library involving the time-varying shadow images, as the preparation for future observations.

ACKNOWLEDGEMENTS

U.M. would like to thank H. Sotani for useful discussions. Works of U.M. are partially supported by JSPS Kakenhi 18K03652 and 22K03623, and President Project (Creative Research) in Akita Prefectural University.

-
- [1] K. Akiyama *et al.* [Event Horizon Telescope], *Astrophys. J. Lett.* **875**, L1 (2019) doi:10.3847/2041-8213/ab0ec7 [arXiv:1906.11238 [astro-ph.GA]].
 - [2] K. Akiyama *et al.* [Event Horizon Telescope], *Astrophys. J. Lett.* **875**, no.1, L2 (2019) doi:10.3847/2041-8213/ab0c96 [arXiv:1906.11239 [astro-ph.IM]].
 - [3] K. Akiyama *et al.* [Event Horizon Telescope], *Astrophys. J. Lett.* **875**, no.1, L3 (2019) doi:10.3847/2041-8213/ab0c57 [arXiv:1906.11240 [astro-ph.GA]].
 - [4] K. Akiyama *et al.* [Event Horizon Telescope], *Astrophys. J. Lett.* **875**, no.1, L4 (2019) doi:10.3847/2041-8213/ab0e85 [arXiv:1906.11241 [astro-ph.GA]].
 - [5] K. Akiyama *et al.* [Event Horizon Telescope], *Astrophys. J. Lett.* **875**, no.1, L6 (2019) doi:10.3847/2041-8213/ab1141 [arXiv:1906.11243 [astro-ph.GA]].
 - [6] K. Akiyama *et al.* [Event Horizon Telescope], *Astrophys. J. Lett.* **910**, no.1, L12 (2021) doi:10.3847/2041-8213/abe71d [arXiv:2105.01169 [astro-ph.HE]].
 - [7] K. Akiyama *et al.* [Event Horizon Telescope], *Astrophys. J. Lett.* **910**, no.1, L13 (2021) doi:10.3847/2041-8213/abe4de [arXiv:2105.01173 [astro-ph.HE]].
 - [8] K. Akiyama *et al.* [Event Horizon Telescope], *Astrophys. J. Lett.* **930**, no.2, L12 (2022) doi:10.3847/2041-8213/ac6674

- [9] K. Akiyama *et al.* [Event Horizon Telescope], *Astrophys. J. Lett.* **930**, no.2, L13 (2022)
doi:10.3847/2041-8213/ac6675
- [10] K. Akiyama *et al.* [Event Horizon Telescope], *Astrophys. J. Lett.* **930**, no.2, L14 (2022)
doi:10.3847/2041-8213/ac6429
- [11] K. Akiyama *et al.* [Event Horizon Telescope], *Astrophys. J. Lett.* **930**, no.2, L15 (2022)
doi:10.3847/2041-8213/ac6736
- [12] K. Akiyama *et al.* [Event Horizon Telescope], *Astrophys. J. Lett.* **930**, no.2, L16 (2022)
doi:10.3847/2041-8213/ac6672
- [13] K. Akiyama *et al.* [Event Horizon Telescope], *Astrophys. J. Lett.* **930**, no.2, L17 (2022)
doi:10.3847/2041-8213/ac6756
- [14] M. Miyoshi, Y. Kato and J. Makino, *Astrophys. J.* **933**, no.1, 36 (2022) doi:10.3847/1538-4357/ac6ddb [arXiv:2205.04623 [astro-ph.HE]].
- [15] J. L. Synge, *Mon. Not. Roy. Astron. Soc.* **131**, no.3, 463-466 (1966)
doi:10.1093/mnras/131.3.463
- [16] J. M. Bardeen, in “Black Holes,” ed. C. DeWitt and B. DeWitt, New York, Gordon & Breach (1973).
- [17] J. P. Luminet, *Astron. Astrophys.* **75**, 228-235 (1979).
- [18] H. Falcke, F. Melia and E. Agol, *Astrophys. J. Lett.* **528**, L13 (2000) doi:10.1086/312423
[arXiv:astro-ph/9912263 [astro-ph]].
- [19] R. Takahashi, *J. Korean Phys. Soc.* **45**, S1808-S1812 (2004) doi:10.1086/422403
[arXiv:astro-ph/0405099 [astro-ph]].
- [20] P. V. P. Cunha, N. A. Eiró, C. A. R. Herdeiro and J. P. S. Lemos, *JCAP* **03**, 035 (2020)
doi:10.1088/1475-7516/2020/03/035 [arXiv:1912.08833 [gr-qc]].
- [21] K. Hioki and U. Miyamoto, *Phys. Rev. D* **78**, 044007 (2008), [arXiv:0805.3146 [gr-qc]].
- [22] C. Bambi and N. Yoshida, *Class. Quant. Grav.* **27**, 205006 (2010) doi:10.1088/0264-9381/27/20/205006 [arXiv:1004.3149 [gr-qc]].
- [23] L. Amarilla, E. F. Eiroa and G. Giribet, *Phys. Rev. D* **81**, 124045 (2010)
doi:10.1103/PhysRevD.81.124045 [arXiv:1005.0607 [gr-qc]].
- [24] L. Amarilla and E. F. Eiroa, *Phys. Rev. D* **87**, no.4, 044057 (2013)
doi:10.1103/PhysRevD.87.044057 [arXiv:1301.0532 [gr-qc]].

- [25] S. W. Wei and Y. X. Liu, JCAP **11**, 063 (2013) doi:10.1088/1475-7516/2013/11/063 [arXiv:1311.4251 [gr-qc]].
- [26] U. Papnoi, F. Atamurotov, S. G. Ghosh and B. Ahmedov, Phys. Rev. D **90**, no.2, 024073 (2014) doi:10.1103/PhysRevD.90.024073 [arXiv:1407.0834 [gr-qc]].
- [27] S. W. Wei, P. Cheng, Y. Zhong and X. N. Zhou, JCAP **08**, 004 (2015) doi:10.1088/1475-7516/2015/08/004 [arXiv:1501.06298 [gr-qc]].
- [28] Z. Stuchlík and J. Schee, Eur. Phys. J. C **79**, no.1, 44 (2019) doi:10.1140/epjc/s10052-019-6543-8
- [29] B. P. Singh and S. G. Ghosh, Annals Phys. **395**, 127-137 (2018) doi:10.1016/j.aop.2018.05.010 [arXiv:1707.07125 [gr-qc]].
- [30] K. Hioki and K. i. Maeda, Phys. Rev. D **80**, 024042 (2009), [arXiv:0904.3575 [astro-ph.HE]].
- [31] A. A. Abdujabbarov, L. Rezzolla and B. J. Ahmedov, Mon. Not. Roy. Astron. Soc. **454**, no.3, 2423-2435 (2015) doi:10.1093/mnras/stv2079 [arXiv:1503.09054 [gr-qc]].
- [32] S. W. Wei, Y. C. Zou, Y. X. Liu and R. B. Mann, JCAP **08**, 030 (2019) doi:10.1088/1475-7516/2019/08/030 [arXiv:1904.07710 [gr-qc]].
- [33] P. Kocherlakota *et al.* [Event Horizon Telescope], Phys. Rev. D **103**, no.10, 104047 (2021) doi:10.1103/PhysRevD.103.104047 [arXiv:2105.09343 [gr-qc]].
- [34] A. Grenzebach, V. Perlick and C. Lämmerzahl, Phys. Rev. D **89**, no.12, 124004 (2014), [arXiv:1403.5234 [gr-qc]].
- [35] S. Abdolrahimi, R. B. Mann and C. Tzounis, Phys. Rev. D **91**, no.8, 084052 (2015), [arXiv:1502.00073 [gr-qc]].
- [36] S. Chandrasekhar, “The mathematical theory of black holes”, Oxford Univ. Press (1992).
- [37] I. D. Novikov and K. S. Thorne, in “Black Holes,” ed. C. DeWitt and B. DeWitt, New York, Gordon & Breach (1973).
- [38] V. P. Frolov and A. Zelnikov, “Introduction to black hole physics”, Oxford Univ. Press (2011).
- [39] D. N. Page and K. S. Thorne, Astrophys. J. **191**, 499-506 (1974).
- [40] M. A. Abramowicz and P. C. Fragile, Living Rev. Rel. **16** (2013), 1 [arXiv:1104.5499 [astro-ph.HE]].
- [41] G. F. R. Ellis, Relativistic Cosmology in “General Relativity and Cosmology,” ed. R. Sachs, Academic Press, New York (1971).